Coalescence-induced jumping of bubbles in shear flow in microgravity

Md Qaisar Raza, Julien Sébilleau, Catherine Colin, Matevz Zupancic, Mattia Bucci, Tadej Troha, Iztok Golobic

Accepted to Phys. Fluids 10.1063/5.0138200

Coalescence-induced Jumping of Bubbles in Shear Flow in Microgravity

Md. Qaisar Raza[1,2], Moritz von Köckritz[1], Julien Sebilleau[1,a)], Catherine Colin[1], Matevz Zupancic[3], Mattia Bucci[3], Tadej Troha[3] and Iztok Golobic[3]

[1]*Université de Toulouse, Institut de Mécanique des Fluides de Toulouse (IMFT), Toulouse 31400, France*

[2]*Department of Mechanical Engineering, National Institute of Technology Patna, Bihar 800005, India*

[3]*University of Ljubljana, Faculty of Mechanical Engineering, Askerceva 6, SI-1000 Ljubljana, Slovenia*

Bubble removal from a solid surface is of significant importance to many technical processes and applications. In addition to the conventional buoyancy aided bubble removal, there is also a passive strategy to remove bubble from a solid surface via coalescence. However, likewise several processes, the coalescence-induced removal of bubbles from the solid surface is masked by the dominant buoyancy, hence, difficult to observe in terrestrial conditions. Microgravity condition offers unique opportunity to investigate such phenomenon in great detail that can significantly improve our fundamental understanding. In this work, we report coalescence-induced jumping of isolated vapor bubbles from the heated substrate during shear flow in microgravity condition. We show that, similar to the coalescence-induced jumping droplets, when two bubbles coalesce, the resulting big coalesced bubble jumps from the substrate due to the conversion of excess surface energy into the translational kinetic energy, which provides the requisite initial velocity for jumping. Jumping of bubbles over a wide range of bubble size (post-coalescence radius $\approx 0.9 - 3.4$ mm) is observed. Bubbles oscillate continuously while rising through certain height post-coalescence. We perform force balance and scaling analysis to develop a model to predict maximum jumping height of bubbles. We show that the jumping height is strongly related to the bubble size and the non-dimensional Ohnesorge number which captures the role of fluid properties governing the coalescence. The physical insights presented in this work have implications for the design of energy systems and microfluidic devices for earth and space-based applications.

I. INTRODUCTION

Bubble lift-off/removal away from the solid surface inside the liquid is of immense importance to a broad range of technical processes and applications such as electrochemical reactions, microfluidics, nuclear reactors, thermal management of electronics, heat exchangers, and energy conversion and storage,[1–9] among others.

a) Corresponding author: Julien Sebilleau, email: julien.sebilleau@imft.fr

For instance, electrochemical reactions encountered in fuel cells and electrolysis processes, including hydrolysis, involves gas evolution reactions (GERs) wherein gas bubbles are formed on the electrode through molecular diffusion processes. The adhesion of gas bubbles to the electrode decreases the area of contact between the electrode and the electrolyte, which impedes the electrolyte diffusion to reduce the mass transfer[3,8]. As a result, speed of the electrochemical reactions is lowered and the system performance is compromised. Therefore, removal of bubbles from the electrode is indispensable for the efficient performance of electro-catalytic GERs. Similarly, adhesion of bubbles on the lenses of underwater camera and surface of diving goggles is undesirable, since it results in poor visibility. Significant research has been focused towards the manipulation of surface roughness and morphology to minimize affinity of bubbles towards the solid surface inside liquid in order to facilitate bubble removal[2,10].

Furthermore, the process of boiling, which is a key to various industrial and household applications, is primarily dictated by the bubble departure/removal away from the heated surface[9,11–13]. Consequently, a great deal of research has been dedicated to investigate the mechanism of bubble departure and its impact on the heat transfer during boiling. Liquid absorbs the latent heat of vaporization to form vapor bubbles on the heated wall followed by its removal due to buoyancy. The recurring process of nucleation of vapor bubble, its growth, departure and rewetting of the heated wall is known as ebullition cycle. Ebullition cycle strongly depends on the buoyancy. Bubble departure is governed by the interplay between various forces such as surface tension, drag, inertia, and buoyancy, among others. Boiling is a very complex phenomenon, since, it involves various physical parameters and mechanisms governing the heat and mass transfer processes such as bubble vaporization, unsteady conduction in the liquid after bubble departure, convection between the nucleation sites. Numerous correlations and models have been developed; however, they are only valid for a specific range of parameters outside which they fail to predict the heat transfer during boiling. Despite extensive studies, boiling is still not understood comprehensively. This may be primarily attributed to the other hidden mechanisms which remains masked by the dominant buoyancy in earth gravity. Among several mechanisms, coalescence-induced departure of bubbles is one such mechanism that has largely remained ignored in the previous boiling studies.

Considerable studies have been performed to investigate the droplet or bubble coalescence[14–16]. The mechanism of bubble coalescence is extraordinarily similar to the droplet coalescence[17,18]. One of the interesting aspects of droplet coalescence is the following: when the two droplets coalesce under favorable conditions, for example, on an ultra-low adhesion nanostructured surface, the resulting coalesced droplet can jump away from the surface even against the

downward acting gravitational force (for upward facing surface). This phenomena is widely reported in the literature as the coalescence-induced droplet jumping[19–23]. The jumping of coalesced droplet is generally attributed to the conversion of excess surface energy into the translational kinetic energy. Accordingly, coalescence-induced jumping droplets have been widely investigated for the enhancement of condensation heat transfer[24–26]. While the phenomena of coalescence-induced jumping droplets are extensively investigated, the study on the coalescence-induced jumping bubbles are rare[27,28]. For example, Soto et al. (2018)[27] numerically and experimentally investigated the coalescence of diffusively growing micron sized ($\sim$600 μm in diameter) CO_2 gas bubbles on the upward facing substrate in earth gravity. Two artificial cavities separated by certain distance, fabricated on the silicon chip, were used to nucleate the gas bubbles. The process of bubble coalescence was analyzed in three phases, namely, neck formation, wave propagation and detachment of bubble. Post-coalescence detachment of bubble was observed. However, in such conditions it is quite complex to isolate the effect of buoyancy from the coalescence-induced detachment. Accordingly, it would be difficult to investigate the true potential of coalescence-induced jumping bubbles in earth gravity. In this regard, microgravity environment can offer an ideal condition to investigate the phenomena of coalescence-induced jumping of bubbles by mitigating the effect of buoyancy. Straub (2001)[29] also reported coalescence-induced bubble departure during boiling on a wire heater in microgravity condition. However, the departure was further complicated by the multiple coalescence events between multiple bubbles formed during boiling.

In this work, we report coalescence-induced jumping of bubbles during boiling with isolated bubbles under the effect of shear flow on a flat heater surface in microgravity environment on-board International Space Station (ISS). In order to investigate the coalescence event, instead of nucleation of two bubbles from two nucleation sites, the experiment was designed to nucleate numerous bubbles from a single artificial nucleation site on the substrate heater under the effect of shear flow. The removal of bubble from the nucleation site due to the shear flow and continuous joule heating of the substrate allowed the nucleation of consecutive bubbles at the same site. This resulted in the formation of a train of sliding bubbles on the heater substrate. When the relative motion between two sliding bubbles gradually decreased, they touch each other, resulting in coalescence, accompanied by the jumping of the resulting big bubble away from the heated surface. Boiling experiments with isolated bubble in shear flow were performed at near-saturated condition and at various heat fluxes, flow rates and pressure conditions. This allowed the investigation of coalescence-induced jumping of two isolated bubbles over a wide range of radius from $\sim 0.7 - 2.9$ mm with a radius ratio of $\sim 0.84 - 1$. The jumping of bubbles is attributed to the release of excess surface energy which manifested as

the kinetic energy of the bubbles. We further show that post coalescence-induced jumping, bubbles continue to oscillate with Minnaert frequency while rising. The jumping height of the bubbles were found to strongly correlate with the size of bubbles. A scaling analysis was performed to develop a model to correlate the jumping height with the bubble radius and Ohnesorge number. We further present guidelines related to the study of the coalescence-induced jumping bubble in future to further improve our fundamental understanding of bubble behavior in microgravity condition.

II. EXPERIMENTAL SETUP AND PROCEDURE

The experimental setup is RUBI (Reference mUltiscale Boiling Investigation) also called "Multiscale Boiling". This is a part of the comprehensive boiling study with isolated bubbles in microgravity conditions on-board the ISS, which has been designed for more than a decade by several European teams involved in the ESA Project BOILING. The primary objective is to mitigate the effect of buoyancy and focus the analysis on the individual isolated bubbles to improve the fundamental understanding of bubble dynamics and heat transfer during boiling.

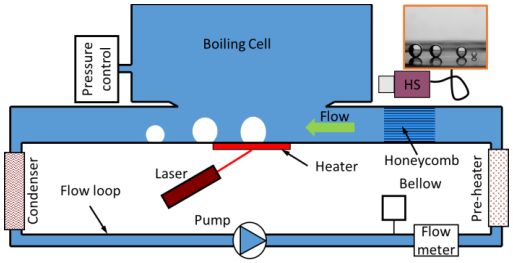

FIG. 1: The schematic representation of the RUBI experimental setup for boiling with isolated bubbles in shear flow.

The schematic of the RUBI setup for performing boiling experiments with isolated bubbles in shear flow is shown in Fig. 1. The experimental setup is composed of an almost cuboid shaped boiling cell which is integrated in a flow loop. The internal dimension of the boiling test cell was approximately $40 \times 40 \times 40$ mm^3. The heater assembly was placed at the bottom of the boiling cell. It consisted of a circular barium fluoride (BaF2) single crystal substrate of 20 mm in diameter and 5 mm in thickness. The substrate was coated with the Chromium Nitride and pure Chromium layers with ~400 nm thickness of each layer using plasma vapor deposition (PVD) technique. The pure chromium layer was present on the top of the substrate and served as a heating element through joule heating. An artificial nucleation site of diameter 30 µm and depth 200 µm was lasered into the center of the substrate. The substrate heater

was further assembled in a Polyetheretherketon (PEEK) cover to form the heater assembly which was fitted at the bottom of the boiling cell and sealed hermetically with the aid of O-rings to avoid any leakages. A laser gun (L404P400M, Thorlabs) capable of delivering output power of 400 mW was used to generate a laser beam of 404 nm wavelength to activate the artificial nucleation site. The flow loop was attached at the bottom of the boiling cell to provide the necessary shear flow over the heater substrate. Flow loop consisted of a gear pump (model FG304XPS24N, Fluid-o-Tech), flowmeter (model FD-SS2A, Keyence) and a honeycomb structure at the inlet of the test cell to ensure proper hydrodynamic conditions. The entrance section of the test cell with the honeycomb has a height of 5 mm. Degassed N-perfluorohexane was used as the test fluid. A bellow was also provided in the loop to account for the volume fluctuation due to the formation of bubbles and also to change the pressure in the test cell. The temperature of the circulating fluid inside the loop was controlled with the aid of a pre-heater and a condenser. Several temperature and pressure sensors were used to monitor the temperature and pressure of the test fluid during the experiments. For more details about the RUBI experimental setup, readers are requested to refer to our previous work[30]. Side view visualization was performed with the aid of a black and white (BW) high-speed camera (model MotionXtra N4, IDT Vision) at 500 fps (frame per second) to capture the bubble dynamics such as bubble growth, its sliding motion and coalescence.

Microgravity boiling experiments with isolated bubbles in shear flow were performed at near-saturated conditions ($\Delta T_{\text{sub}} = 3$ °C and 5 °C, $\Delta T_{\text{sub}} = T_{sat} - T_{liquid}$, where T_{sat} is the saturation temperature and T_{liquid} is the liquid bulk temperature). Prior to start of the boiling experiments, the required flow rate and the temperature of the liquid was stabilized. The joule heating of the heater substrate was initiated to maintain a constant heat flux (q") on the substrate surrounding the nucleation site. After certain waiting time t_{wait}, laser gun was used to trigger a laser pulse which activated the nucleation site by providing necessary wall superheat for bubble nucleation. It should be noted that only the first bubble was nucleated with the help of laser pulse. Once the nucleation site became active, bubbles nucleated after sliding of previous bubble due to shear flow. In microgravity, the growth rate and size of the bubble is primarily governed by evaporation at the bubble foot which depends on the thickness of the superheated layer adjacent to the heated wall. Accordingly, boiling was performed over a wide range of experimental conditions, resulting in varying thickness of superheated layer, hence, coalescence of a wide range of bubble radius ($\sim 0.7 - 2.9$ mm) was observed. Experiments were performed at various heat fluxes q" (0.5 W/cm^2, 0.75 W/cm^2, and 1 W/cm^2), t_{wait} (2 s, 5 s, and 10 s), flow rates (low $\approx$ 100 ml/min, medium $\approx$ 300 ml/min, and high $\approx$ 500 ml/min), and pressure p (500 mbar, 750

mbar, and 1000 mbar). However, it should be noted that the properties of the fluid governing the bubble coalescence do not change significantly at different pressures (see Table 1).

TABLE I. Properties of the fluid at saturated condition and at different pressures.

S.N.	Pressure	$\rho_l\ (kg/m^3)$	$\mu\ (Pa.s)$	$\sigma\ (N/m)$
1.	$1000\ mbar$	1619.82	0.000453	0.00827
2.	$750\ mbar$	1634.54	0.000490	0.00897
3.	$500\ mbar$	1653.91	0.000549	0.00991

The images of the bubble obtained through shadowgraph using BW camera were digitized with the aid of the in-house developed Matlab-based image processing code. The bubble contour was detected with the help of various steps of the image processing analysis, such as contrast adjustment, image inversion, binarization, filtering, filling of holes in the bubble, segmentation of unwanted area, boundary detection and tracing. After determination of the bubble contour several geometrical parameters, for example, bubble radius (R), the x and y co-ordinates of the center of gravity (X and Y) of the bubbles, and contact angles were estimated. For more details on the image processing readers are requested to refer our previous work[31].

Uncertainty analysis. The bubble size estimation depends on the detection of the bubble contour. Incorrect detection in the bubble contour can lead to the deviation in the bubble size. The maximum uncertainty in the bubble size is found to be less than 40μm. The incorrect identification of the contact points at the bubble base also leads to the uncertainty in measurement of contact angle. The maximum uncertainty in the contact angle was found to be less than 6°. The maximum uncertainty in the center of gravity (CG) identification was within ±1 pixel with the image resolution of 20μm/pixel. The associated uncertainty in the jumping height was estimated to be less than 0.2 mm. The curve fitting of the y-coordinate of the CG location, post-jumping of bubbles, resulted in measurement uncertainty in the jumping velocity (U_j). The uncertainty in the frequency (f) of oscillation of the bubble was calculated as the average difference between manually calculated frequency and frequency calculated using FFT (Fast Fourier Transform). Furthermore, error propagation analysis was performed to evaluate the uncertainty associated with the excess surface energy (E_s), kinetic energy (E_k), non-dimensional coalescence time (t^*), and energy conversion efficiency (η), among others. These uncertainties are displayed as error bars in the figures.

III. RESULTS AND DISCUSSION

A. Jumping Bubble

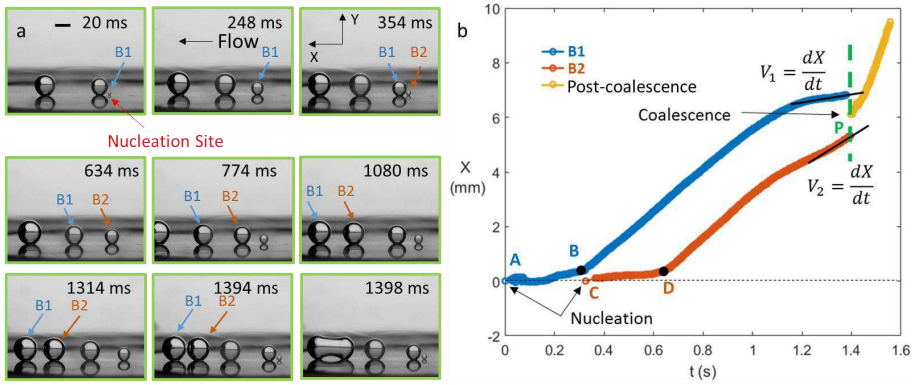

FIG. 2: (a) The time-lapse images of sliding bubbles during boiling with isolated bubble in shear flow in microgravity condition. The scale bar corresponds to 1 mm length. Bubble B1 nucleates at time $t = 0$ ms. (b) Variation of the x-coordinate of the center of gravity with time for the bubble B1 and B2.

The time-lapse images of a train of sliding bubbles during boiling in shear flow is shown in Fig. 2(a) ($q" = 0.75$ W/cm^2, $Q = 500$ ml/min, $p = 1000$ mbar, and $\Delta T_{sub} = 5$ °C). The nucleation site was activated with the laser pulse, resulting in the nucleation of bubble. Bubble grew to a particular size and detached from its position and continued to slide on the heated wall under the influence of shear flow. This allowed the nucleation of next bubble at the nucleation site and the cycle continued. When the relative motion of two consecutive bubbles [B1 and B2, Fig. 2(a)] during sliding gradually decreased, they come close enough to touch each other, resulting in coalescence [image corresponding to 1398 ms, Fig. 2(a)].

The variation of x-coordinates of the center of gravity with time for the bubbles B1 and B2 are shown in Fig. 2(b). Points A and C correspond to the nucleation of bubbles B1 and B2, respectively. After nucleation, bubble B1 continues to grow at the nucleation site, as evident from the almost constant value of x-coordinate in the region AB (blue color line). At point B, bubble B1 starts sliding and beyond that it continues to slide with the velocity $V_1 = dX/dt$, which is clear from the increased slope of the curve (blue color line). The sliding/detachment of bubble B1 away from the nucleation site is followed by the nucleation of new bubble B2 (point C). Similar to the bubble B1, Bubble B2 also starts sliding after point D due to the drag force exerted by the shear flow. The corresponding temporal variation of bubble radius for both the bubbles is shown in Fig. 3(a). Bubbles continue to grow at the nucleation site (region AB

and CD) as well as during sliding motion (BP and DP) on the heater substrate as evident from the gradual increase in the bubble diameter with time, since the substrate was maintained at a constant heat flux. The evolution of bubble radius with time followed the relation $R \propto t^{0.5}$, which is a characteristic of the bubble growth controlled by the heat-diffusion[32].

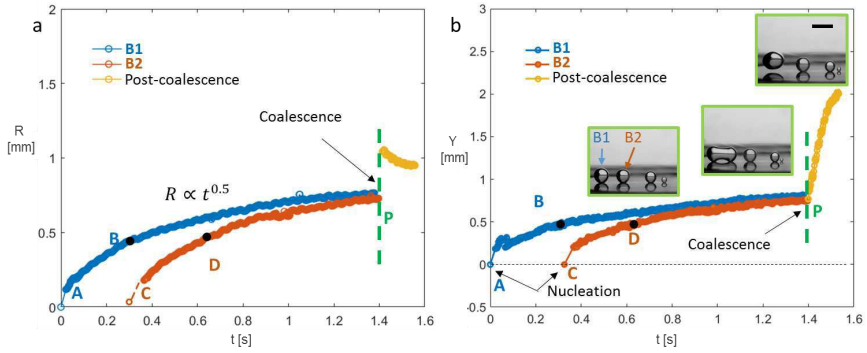

FIG. 3: (a) Temporal evolution of bubble radius before and after coalescence. (b) The corresponding variation of y-coordinated of the CG with time. The vertical green color dashed line indicates the event of coalescence. The scale bar in the inset image corresponds to 2 mm.

When the two bubbles B1 and B2 came closed enough to touch each other due to the decrease in the relative velocity of approach ($V_1 - V_2$), coalescence occurred [the green color vertical dashed line in Fig. 3(a) and 3(b)]. Interestingly, coalescence also resulted in the jumping of the coalesced bubble [inset image Fig. 3(b)], as evident from the sudden increase in the y-coordinate of the center of gravity of the bubble post-coalescence (Fig. 3b). The bubble size significantly increased post-coalescence. The slight decrease in bubble size post-coalescence induced jumping [yellow color data points, Fig. 3(a)] can be attributed to the condensation as liquid was maintained under subcooled condition ($\Delta T_{\text{sub}} = 5\ ^{\circ}\text{C}$). After jumping vertically, bubble continued to move along the flow direction [yellow color data points, Fig. 2(b)]. The mechanism of bubble coalescence is discussed next.

B. Coalescence Mechanism

The schematic representation of the bubble coalescence is shown in Fig. 4(a). The corresponding real time-lapse images of the coalescence of two different size of bubble pairs is shown in Fig. 4(b) and 4(c). When the liquid-vapor interfaces of the two bubbles make contact, coalescence initiated with the development of a neck or vapor-bridge between them [Fig. 4(a) I, image corresponding to t^*~0.21 in Fig. 4(b) and t^*~0.06 in Fig. 4(c), where, t^* ($= \frac{t}{\tau_{cap}}$)

is the actual time normalized with the capillary time scale $\tau_{cap} = \sqrt{\frac{\rho_l R^3}{\sigma}}$ of the bubble]. The neck radius grows very rapidly with time which is driven by the Laplace pressure ΔP caused by the curvature difference between the neck $(1/r_n)$ and the bubble $(1/R)$, $\Delta P \sim \frac{\gamma R}{r_n^2}$. The initial state of the coalescence up to a critical value of neck radius lies in the inertially limited viscous regime (ILV), wherein the viscosity of the fluid inside the bubble controls the development of the neck region irrespective of the density and viscosity of fluid outside the bubble[18]. However, this regime exists for a very short period. The corresponding critical value of the neck radius ($r_{n,c} = 2.8\mu_{in}\sqrt{R/\rho_l\sigma}$, where μ_{in} is the viscosity of the vapor inside bubble, and ρ_l and σ is the density and the surface tension of the liquid, respectively) is found to be of the order of $\sim$400 nm for bubble radius of 1 mm. Afterwards, the coalescence is transitioned to the outer-fluid inertia dominated regime or the outer-fluid viscosity dominated regime depending on the value of Ohnesorge number $Oh = \mu_l/\sqrt{\rho_l\sigma R}$, where, μ_l is the viscosity of liquid. For low viscosity fluids (or $Oh < 0.3$), inertia dominates at late time and the inertia stress balancing the Laplace pressure scaled as $\rho U^2 \sim \rho \dot{r_n}^2$. Whereas for high viscosity fluids (or $Oh > 0.3$), outer-fluid viscosity dominates at late time and the viscous stress scales as $\mu\frac{\dot{r_n}}{r_n}$ [18]. In the present work, Oh estimated to be $\sim 2.2 \times 10^{-3} - 4.1 \times 10^{-3}$ for entire range of the bubble, indicating inertia dominated regime during coalescence.

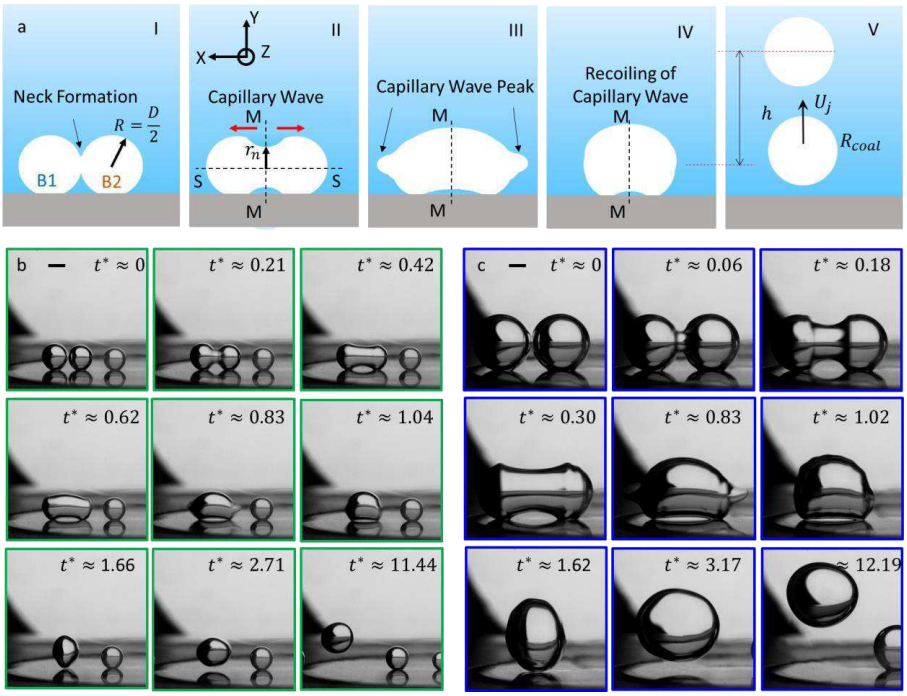

FIG. 4: (a) The schematics of the bubble coalescence event. The time-lapse images of the bubble coalescence events at (b) q'' = 0.75 W/cm^2, Q = 500 ml/min, p = 1000 mbar, ΔT_{sub} = 5 °C and (c) q'' = 1 W/cm^2, Q = 100 ml/min, p = 1000 mbar, ΔT_{sub} = 5 °C. The scale bar corresponds to 1 mm.

In the inertia dominated regime the neck radius r_n of the bubble evolve with time during coalescence through the following relation[18,28,33].

$$\frac{r_n}{R} = C\sqrt{t^*} \tag{1}$$

where, C is the non-dimensional constant and reported to be 1.4 in the literature for the bubble coalescing in the stagnant liquid[18,28]. The plot of the dimensionless neck radius ($\frac{r_n}{R}$) versus $\sqrt{t^*}$ is shown in Fig. 5(a). The good match between the experimental data and the Equation (1), suggests a good agreement between the coalescence of bubble during shear flow in microgravity and terrestrial condition reported in the literature[18,28]. The deviation from the Equation (1) at later times can be attributed to the finite size effect of the bridge radius, which becomes more important as the neck radius approaches size of the bubble[18,33].

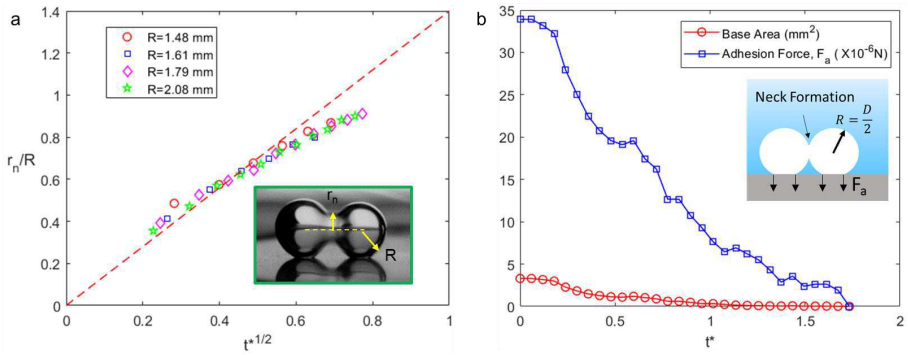

FIG. 5: (a) Variation of dimensionless neck radius versus square root of non-dimensional time. (b) Variation of bubble base area (red color circular symbols) and adhesion force (blue color square symbols), corresponding to bubble coalescence in Fig. 4(c), versus non-dimensional time.

The process of neck formation generates a capillary wave that traverse along the liquid-vapor interface away from the neck region [Fig. 4(a) II, images at $t^*\sim0.42$ and $t^*\sim0.62$ in Fig. 4(b) and images at $t^*\sim0.18$ and $t^*\sim0.30$ in Fig. 4(c)]. When the capillary wave reaches at the opposite ends of the bubble to form peak [Fig. 4a III, $t^*\sim0.83$ in Fig. 4(b), and Fig. 4(c)], it is reflected back towards the central symmetry plane (MM) of the coalescing bubble [Fig. 4(a) IV, $t^*\sim1.04$ in Fig. 4(b), and $t^*\sim1.02$ in Fig. 4(c)]. The propagation of capillary wave significantly alters the bubble contact line to reduce the base area during coalescence [red color circular symbols, Fig. 5(b)]. Consequently, the adhesion force acting on the bubble vanishes [blue color square symbols, Fig. 5(b)]. Moreover, the propagation of capillary wave at the interface may also induce non-negligible flow in the liquid around the bubble with considerable momentum. The component of the momentum in the x and z direction parallel to surface SS gives zero net momentum due to the symmetry. However, due to the non-symmetrical nature (presence of wall at the bottom) of the coalescence process about the horizontal surface SS [Fig. 4(a) II], there is a net component of this momentum in the y-direction normal to the symmetry breaking surface SS[20], which provides the necessary initial kinetic energy for the jumping of bubbles [Fig. 4(a) V, $t^*\sim1.66$ in Fig. 4(b), and $t^*\sim1.62$ in Fig. 4(c)].

The plot of the non-dimensional time at lift-off t_j^* versus pre-coalescence bubble size is shown in Fig. 6(a). The average value of non-dimensional time at lift-off $t_{j\,avg}^*$ of the coalesced bubble from the heater surface was found to be $\approx 1.6 \pm 0.24$ for the entire range of bubble size under different flow rate conditions, which indicates an insignificant effect of flow rate on the dynamics of bubble coalescence before lift-off. At the point of lift-off, a value

of $t_j^* = 1.8$ is reported in the literature for bubble coalescence in terrestrial condition[28]. A similar range of values of t_j^* in this work and in the literature suggests an insignificant role of gravity during coalescence of bubbles before lift-off.

Furthermore, it should be noted that when the capillary wave peaks are formed [Fig. 4(a) III and Fig. 6(b) inset image], the pinch-off of the satellite bubble was not observed despite surface tension dominating over the viscosity, as evident from the low value of $Oh \sim 10^{-3}$. This was in contrast to the bubble and droplet coalescence reported in the literature[34–37]. The absence of pinch-off of the satellite bubble may be attributed to the presence of wall at the bottom, which perturbed the propagation of capillary wave along the bottom half of the bubble. Consequently, axis-symmetry of the peak about line SS [Fig. 4(a) III and Fig. 6(b) inset image] is broken and it did not result in the formation of secondary neck to pinch off the satellite bubble. The plot of the non-dimensional time when the capillary wave peaks are formed (t_p^*) versus the average bubble size pre-coalescence (R) at various flow rates is shown in Fig. 6(b). The average value of t_p^* is found to be $\approx 0.77 \pm 0.07$ which in agreement with the bubble coalescence reported in literature[35].

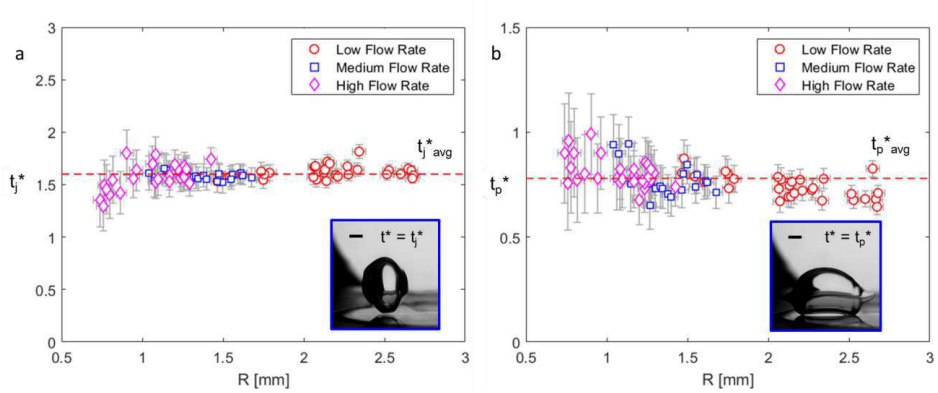

FIG. 6: (a) The variation of non-dimensional time at lift-off of bubble from the substrate with average bubble size pre-coalescence. (b) The variation of non-dimensional time when the capillary wave reaches the peak position [Fig. 4(a) III] with average bubble size pre-coalescence. Horizontal dashed line represents the average value. Scale bar in the inserts represents 1mm.

Post lift–off from the heater surface, bubble rise with kinetic energy with initial jumping velocity U_j [Fig. 4(a) V]. Jumping of bubbles due to coalescence can be attributed to the liberation of excess energy (E_s) which transformed

into the kinetic energy (E_k) of the bubble post coalescence at lift-off[27]. Excess energy (E_s) is estimated as total change in interfacial energy before and after coalescence of the bubbles.

$$E_k = \frac{1}{2} C_{AM} \rho_l \frac{4}{3} \pi R_{coal}^3 U_j^2 \quad (2)$$

$$E_s = (A_1 + A_2)\sigma - A_{coal}\sigma + (a_1 + a_2)\sigma cos\theta \quad (3)$$

where, R_{coal} is the equivalent radius of the bubble at lift-off [Fig. 4(a) V], A_1 and A_2 are the liquid-vapor interfacial area, a_1 and a_2 are the base area of the bubble before coalescence, A_{coal} is the liquid-vapor interfacial area of the bubble post lift-off from the surface, θ is the contact angle and $C_{AM} = 0.803$ is the added mass coefficient for spherical bubble close to the wall.

The plots of excess energy (E_s) and kinetic energy (E_k) for various bubble sizes are shown in Fig. 7(a) and 7(b). The excess and the kinetic energy both increased with the increase in the bubble size. Please note that for a given size of bubble, the magnitude of the kinetic energy is significantly smaller than the excess energy. The plot of the energy conversion efficiency $\eta = E_k/E_s$ during coalescence versus bubble size is shown in Fig. 7(c). The process of coalescence is an inefficient process, only a small portion of the excess energy is converted into the translational kinetic energy of the jumping bubble. The value of the initial kinetic energy of jumping bubble post-coalescence is estimated to be around ≈ 5 % of the excess energy [Fig. 7(c)], which is similar to the coalescence-induced jumping droplets reported in the literature[20,38–40]. Accordingly, jumping velocity of the bubbles (U_j) was found to be related to the inertia-capillary driven velocity ($U \sim \sqrt{\sigma/\rho_l R_{coal}}$) through the relation $U_j \approx 0.24U$ [Fig. 7(d)] which also agrees with the coalescence induced jumping droplets[20,39].

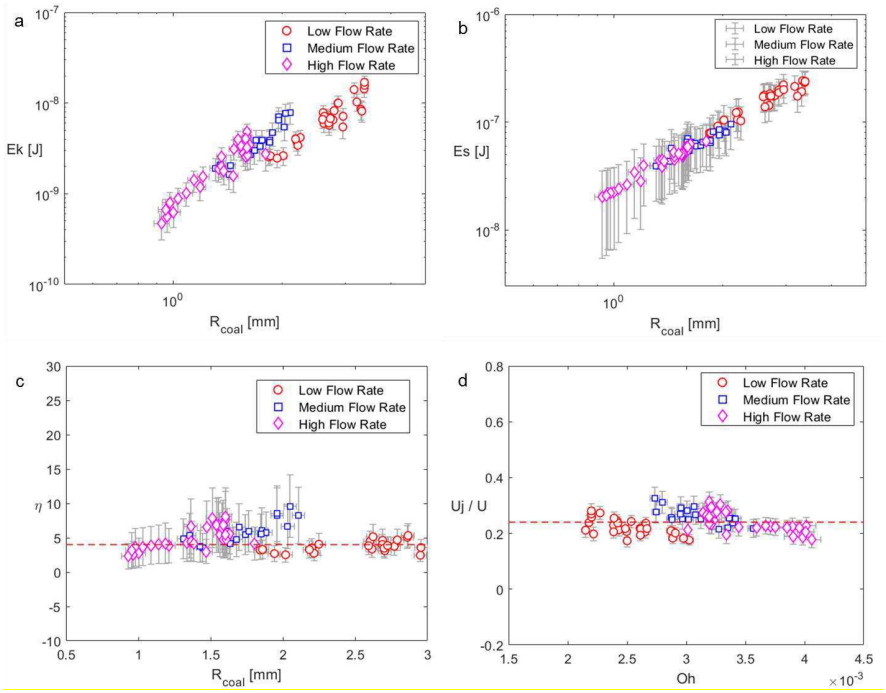

FIG. 7: (a) The plot of kinetic energy versus post-coalescence bubble radius at lift-off, (b) variation of excess surface energy of bubble versus post-coalescence bubble radius at lift-off, (c) the energy conversion efficiency, i.e., the ratio of E_k and E_s, versus the bubble size at lift-off, (d) the plot of ratio of jumping velocity to the inertia-capillary driven velocity versus the Ohnesorge number corresponding to the bubble size shown in (a), (b) and (c). Horizontal dashed line indicates average value.

The plot of jumping velocity U_j versus bubble radius at lift-off R_{coal} is shown in Fig. 8. The inertia-capillary driven velocity ($U \sim \sqrt{\sigma/\rho_l R_{coal}}$) decreases with the increase in the bubble size, accordingly, jumping velocity U_j was observed to decrease with the increase in the bubble size.

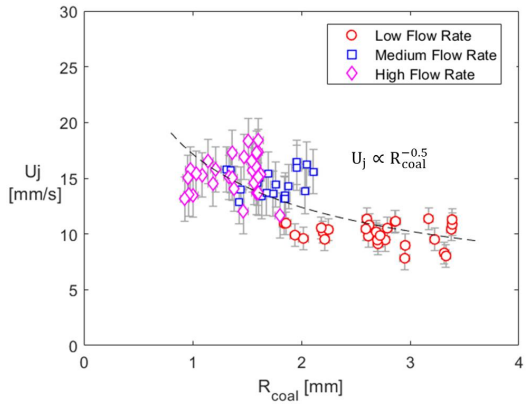

FIG. 8: Variation of initial jumping speed (U_j) with radius of bubbles post-coalescence (R_{coal}).

C. Oscillation of Bubble

The time-lapse images of the bubble post lift-off from the substrate is shown in Fig. 9. The coalesced bubble oscillates strongly under the effect of inertia due to the capillary wave while rising away from the substrate. It first elongated vertically then horizontally. In order to capture the oscillation behavior, we plotted the variation of non-dimensional bubble radius in horizontal (R_x/R_{coal}) and vertical plane (R_y/R_{coal}) with respect to time, shown in Fig. 10(a). The initial amplitude of oscillation in horizontal plane is found to be relatively higher than the vertical plane that may be attributed to the rising motion of bubble. Moreover, presence of local maxima in the curve indicates the presence of various modes of oscillation, Fig. 9 and Fig. 10(a).

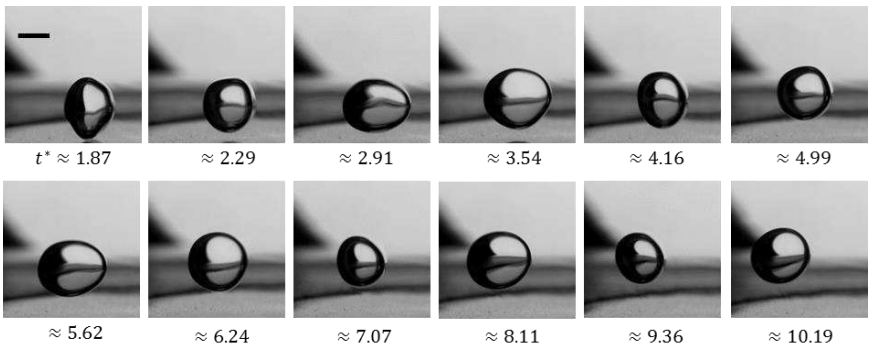

FIG. 9: Time-lapse images of bubble oscillation post lift-off from the substrate. Scale bar represents 1 mm.

We also performed the FFT (Fast Fourier Transform) of the signal, shown in Fig. 10(a), to quantify the most dominant frequency of oscillation. The plot of the corresponding frequency of oscillation f versus bubble size at lift-off (R_{coal}) is shown in Fig. 10(b). The frequency f was found to be related with the bubble size through the relation $f \sim {R_{coal}}^{-1.5}$, which is in agreement with the correlation[41] for single oscillating bubble $(2\pi f)^2 = (n-1)(n+1)(n+2)\sigma/\rho {R_{coal}}^3$, where n is the mode of oscillation. This correlation is related to the well-known Minnaert frequency[42]. We back calculated n and found its value to be ≈ 2, indicating the most dominant mode of oscillation while damping of higher modes of oscillation can be attributed to the viscous effect.

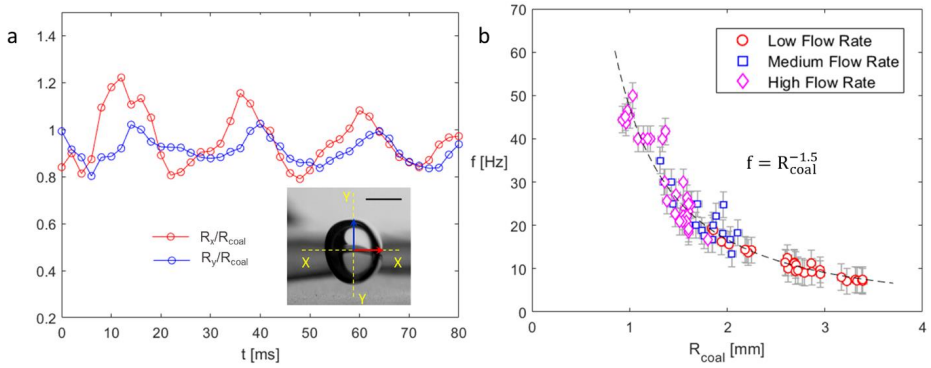

FIG. 10: (a) Variation of non-dimensional bubble radius in horizontal (R_x/R_{coal}) and vertical (R_y/R_{coal}) direction during oscillation post lift-off versus time. Inset image is a representative image of the oscillating bubble post lift-off. Scale bar represents 1 mm. (b) The variation of frequency of oscillation with bubble radius at lift-off.

In order to compare the oscillation behavior of various size of bubbles, we plotted the non-dimensional radius in horizontal direction (R_x/R_{coal}) versus non-dimensional time during oscillation; the corresponding plot is shown in Fig. 11. There was almost similar oscillation pattern for the different sized bubbles at different flow rate conditions, thus, exhibiting insignificant effect of flow rates on the bubble oscillation. Additionally, the amplitude of the dimensionless radius decreased continuously with time, which can be attributed to the cumulative effect of viscous damping and condensation due to liquid subcooling. It should be noted that we could not captured the complete damping of the oscillation, as the bubbles moved quickly out of the viewing zone due to the shear flow. We further perform force balance analysis to develop a model to predict the jumping height of the bubble and is presented next.

Accepted to Phys. Fluids 10.1063/5.0138200

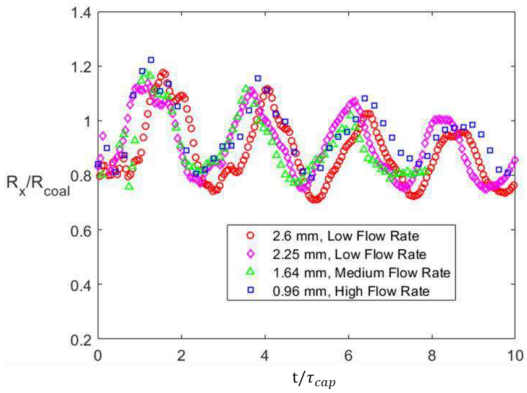

FIG. 11: Variation of non-dimensional bubble radius (R_x/R_{coal}) during oscillation versus time normalized with respect to capillary time scale for different bubble size R_{coal} at lift-off.

D. Modeling of Jumping Height

Post jumping, bubbles continue to move under the influence of shear flow. The variation of x-coordinate of the bubble after lift-off from the substrate for various flow rate conditions is shown in Fig. 12(a) and the liquid velocity profile above the heater substrate is also shown in Fig. 12(b). Numerical simulations of the flow in the preheater, entrance section with the honeycomb and test section have been performed with the software OpenFOAM in steady and transient conditions in laminar flows. Unlike the coalescence event before jumping, the liquid flow rate has a significant effect on the bubble dynamics after jumping. At the low flow rate, bubbles translated with relatively small velocity in comparison to the higher flow rate due to the low value of the drag, as evident by the more time taken by the bubble while translating through the same distance.

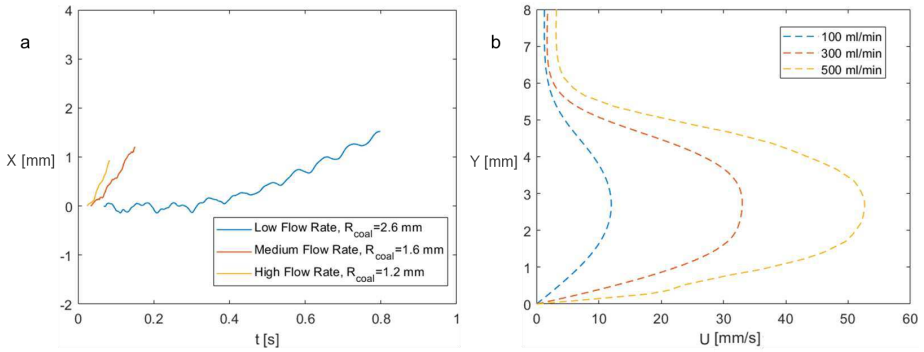

FIG. 12: (a) The temporal variation of X co-ordinate of the bubble post-jumping from the substrate. (b) The liquid velocity above the substrate estimated using numerical simulation at different shear flow rate conditions.

The variation of jumping height h of the bubble with time post-jumping at various flow rate conditions is shown in Fig. 13(a) (solid line). Jumping height h is calculated as the difference between the CG height of the bubble after coalescence and the average CG height of the bubble before coalescence. The fluctuation in the jumping height can be attributed to the oscillation of CG of the bubble post jumping. At low flow rate condition, the jumping height gradually increase followed by saturation at h_{max}, due to the continuous drag force experienced by the bubble while rising in the vertical direction. However, at high and medium flow rate conditions, bubbles quickly move out of the viewing zone under the influence of shear flow and the saturation of jumping height or h_{max} could not be captured.

Considering the motion of the bubble only in the vertical plane [Fig. 13(b)], the forces experienced by the bubble are the added mass force F_{AM} and the drag force F_D. Therefore, the force balance can be written as follows.

$$F_{AM} + F_D = 0 \tag{4}$$

$$C_{AM}\rho_l V_B \frac{dU_h}{dt} + \frac{1}{2}\rho_l C_D \pi R_{coal}^2 U_h^2 = 0 \tag{5}$$

where, C_{AM} is the added mass coefficient, $V_B = \frac{4}{3}\pi R_{coal}^3$ is the bubble volume post jumping, U_h is the instantaneous velocity in vertical direction $U_h = \frac{dh}{dt}$, $C_D = \frac{48}{Re}$ is the drag coefficient as proposed by Levich[43]. Equation (5) reduces to

$$C_{AM}\rho_l \frac{4}{3}\pi R_{coal}^3 \frac{d^2h}{dt^2} + 12\pi\mu R_{coal}\frac{dh}{dt} = 0$$

$$\frac{d^2h}{dt^2} = -\alpha\frac{dh}{dt} \tag{6}$$

where, $\alpha = \frac{9\mu}{C_{AM}\rho_l R_{coal}^2}$. Double integrating the equation (6) with boundary condition at $t = 0, h = 0$ and , $U_h = U_j$, we get,

$$h = \frac{U_j}{\alpha}(1 - e^{-\alpha t}) \tag{7}$$

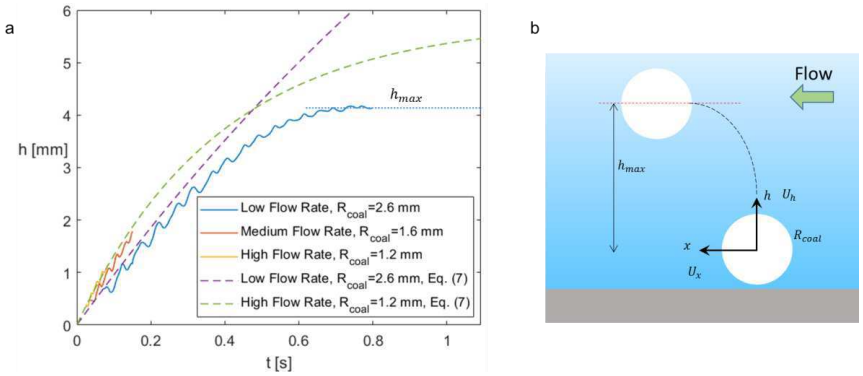

FIG. 13: (a) The temporal variation of CG height of the bubble in shear flow at different liquid flow rate conditions post jumping of the bubbles from the substrate. (b) The schematic of the rising motion of the bubble post jumping.

The comparative plot of the theoretical (dashed line) and actual (solid line) variation of height with time post jumping of the bubbles are shown in Fig. 13(a). The actual value of maximum jumping height h_{max} is found to be smaller than the theoretical value which may be due to the increased energy losses due to the oscillation of the bubble post lift-off [Fig. 10(a)]. However, under limiting condition, i.e., $t \to \infty$, equation (7) suggests that the maximum jumping height should be scaled as follows.

$$h_{max} \propto \frac{U_j}{\alpha}$$

$$h_{max} \propto 0.24\sqrt{\frac{\sigma}{\rho_l R_{coal}}}\,\frac{C_{AM}\rho_l R_{coal}^2}{9\mu} \propto \frac{\sqrt{\sigma\rho_l}}{\mu} R_{coal}^{3/2}$$

$$h_{max} \propto \frac{R_{coal}}{Oh} \tag{8}$$

where, $Oh = \mu_l/\sqrt{\rho_l \sigma R}$ is the Ohnesorge number. The equation (8) suggests that the jumping height of the bubble is directly related with the bubble radius and inversely related to the Ohnesorge number which captures the fluid properties in terms of viscous, inertia and surface tension forces. Inertia and surface tension forces facilitate jumping of bubbles whereas viscosity has an adverse effect on the jumping height. In the present work, the properties of the fluid do not changes significantly over the entire range of working condition (see Table 1). Therefore, equation (8) reduces to the following form.

$$h_{max} \propto R_{coal}^{1.5} \tag{9}$$

The log-log plot of the jumping height h_{max} versus bubble radius R_{coal} is shown in Fig. 14. The value of the exponent was found to be 1.5 with a proportionality constant of ≈ 0.9. The relatively small value of jumping height in the present work in comparison to the theoretical value [dashed line, Fig. 13(a)], may be attributed to several effects: the presence of flow, the condensation of the bubble after jumping and the dissipation of energy by the oscillation of the bubble as seen in Fig. 10(a). These effects have not been taken into account in our scaling analysis.

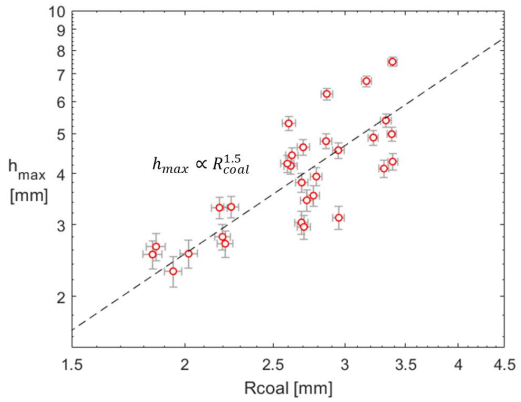

FIG. 14: Log-log plot of maximum jumping height versus bubble radius R_{coal} at lift-off at low flow rate condition.

We anticipate likewise the coalescence-induced jumping droplet, the coalescence-induced jumping bubble will also depend on the wettability of the surface. Accordingly, it would be interesting to investigate the effect of surface wettability on jumping of bubbles. Additionally, the above experiment may be performed in a pool of stagnant liquid at saturated condition (for vapor bubble) or subcooled liquid condition with the gas bubbles where the effect of flow field and condensation would be completely absent. This will enable us to understand the true potential of coalescence-induced jumping of bubbles. Moreover, the coalescence-induced jumping of bubbles also has implications for the enhancement of heat transfer during boiling. For instance, few studies report significantly high heat flux during bubble coalescence due to the transient conduction and improved rewetting caused by the oscillation of the contact line and microlayer[44]. This mechanism of bubble departure must also be taken into account during flow boiling in terrestrial conditions in order to accurately predict the heat transfer performance.

IV. CONCLUSIONS

In summary, we have pointed out coalescence-induced jumping of vapor bubbles during boiling with isolated bubble in shear flow in microgravity condition. Such phenomena is rare to observe in the earth gravity due to the dominant role of buoyancy, which detaches the bubbles before coalescence. Boiling experiments were performed in shear flow to nucleate numerous bubbles from a single nucleation site which enabled us to investigate the coalescence-induced jumping over a wide range of bubble size. Jumping of bubble is attributed to the liberation of excess surface energy due to coalescence. The effect of the flow rates on the dynamics of bubble coalescence before lift-off as well as bubble oscillation post lift-off was not significant. Furthermore, scaling analysis is performed to develop a correlation to predict the maximum jumping height of the bubble based on the bubble size. The maximum jumping height of the bubble due to the coalescence-induced jumping was directly related to the bubble radius at lift-off through an exponent of 1.5. Moreover, a considerable similarity was also observed between jumping of bubbles in microgravity and jumping of droplets in terrestrial conditions. Guidelines are also proposed for the future studies related to the coalescence-induced jumping of bubbles to further improve our fundamental understanding. We believe that the physical insights presented in this work have implications in several industrial processes and applications including boiling heat transfer for terrestrial and microgravity applications.

Acknowledgements

The authors would like to thank the European Space Agency ESA for its support in the MAP Boiling Project and the development and coordination of the Multiscale Boiling Experiments. The French space agency CNES is acknowledged for the post-doc grant of Md. Qaisar Raza and its support in the frame of the GDR "Micropesanteur Fondamentale et Appliquée". Authors from University of Ljubljana would like to acknowledge the financial support from the Slovenian Research Agency: research core funding No. P2-0223.

References

[1] C. Yu, P. Zhang, J. Wang, and L. Jiang," Superwettability of Gas Bubbles and Its Application: From Bioinspiration to Advanced Materials", Adv. Mater. **29**, 1703053 (2017).

[2] J. Yong, F. Chen, Y. Fang, J. Huo, Q. Yang, J. Zhang, H. Bian, and X. Hou, " Bioinspired Design of Underwater Superaerophobic and Superaerophilic Surfaces by Femtosecond Laser Ablation for Anti- or Capturing Bubbles", Appl. Mater. Inter. 9, 39863-39871 (2017).

[3] S.K. Mazloomi and N. Sulaiman, "Influencing factors of water electrolysis electrical efficiency", Renew. Sust. Energ.

Rev. **16**, 4257-4263 (2012).

[4] S. Shibata, "Supersaturation of oxygen in acidic solution in the vicinity of an oxygen-evolving platinum anode", Electrochim. Acta **23**, 619-623 (1978).

[5] L. Mueller and M. Krenz, "On the relation between the transport of electrochemically evolved Cl2 and H2 into the electrolyte bulk by convective diffusion and by gas bubbles", Electrochim. Acta **34**, 305-308 (1989).

[6] J.P. Glas and J.W. Westwater, "Measurements of the growth of electrolytic bubbles", Int. J. Heat Mass Tran. **7**, 1427-1443 (1964).

[7] Z. Lu, W. Zhu, X. Yu, H. Zhang, Y. Li, X. Sun, X. Wang, H. Wang, J. Wang, J. Luo, X. Lei, and L. Jiang, "Ultrahigh hydrogen evolution performance of under-water "superaerophobic" MoS2 nanostructured electrodes", Adv. Mater. **26**, 2683-2687 (2014).

[8] W. Xu, Z. Lu, X. Sun, L. Jiang, and X. Duan, "Superwetting electrodes for gas-involving electrocatalysis", Accounts Chem. Res. **51**, 1590-1598 (2018).

[9] M.Q. Raza, N. Kumar, and R. Raj, "Surfactants for bubble removal against buoyancy", Sci. Rep. **6**, 19113 (2016).

[10] J.E. George, S. Chidangil, and S.D. George, "Recent progress in fabricating superaerophobic and superaerophilic surfaces", Adv. Mater. Interfaces **4**, 1601088 (2017).

[11] R. Cole, "Bubble frequencies and departure volumes at subatmospheric pressures", AIChE Journal **13**, 779-783 (1967).

[12] N. Kumar, Q. Raza, and R. Raj, "Surfactant aided bubble departure during pool boiling", Int. J. Therm. Sci. **131**, 105-113 (2018).

[13] N. Zuber, "Nucleate boiling. The region of isolated bubbles and the similarity with natural convection", Int. J. Heat Mass Tran. **6**, 53-78 (1963).

[14] A.L. Xing, B.J. Li, C.M. Jiang, and D.L. Zhao, "Simulation of coalescence dynamics of droplets on surfaces with different wettabilities", Phys. Fluids **34**, 072114 (2022).

[15] M. Kumar, R. Bhardwaj, and K.C. Sahu, "Coalescence dynamics of a droplet on a sessile droplet", Phys. Fluids **32**, 012104 (2020).

[16] T. Li, A.M. Zhang, S.P. Wang, G.Q. Chen, and S. Li, "Nonlinear interaction and coalescence features of oscillating bubble pairs: Experimental and numerical study", Phys. Fluids **31**, 092108 (2019).

[17] F.H. Zhang, M.-J. Thoraval, S.T. Thoroddsen, and P. Taborek, "Partial coalescence from bubbles to drops", J. Fluid Mech. **782**, 209-239 (2020).

[18] J.D. Paulsen, R. Carmigniani, A. Kannan, J.C. Burton, and S.R. Nagel, "Coalescence of bubbles and drops in an outer fluid", Nat. Commun. **5**, 3182 (2014).

[19] J.B. Boreyko and C.-H. Chen, "Self-propelled jumping drops on superhydrophobic surfaces", Phys. Fluids **22**, 091110 (2010).

[20] R. Enright, N. Miljkovic, J. Sprittles, K. Nolan, R. Mitchell, and E.N. Wang, "How coalescing droplets jump", ACS Nano **8**, 10352-10362 (2014).

[21] S.J. Lee, S. Lee, and K.H. Kang, "Droplet jumping by electrowetting and its application to the three-dimensional digital microfluidics", Appl. Phys. Lett. **100**, 81604 (2012).

[22] B. Li, F. Xin, W. Tan, and G. Zhu, "A new theoretical model for coalescence-induced droplet jumping on hydrophobic fibers", Ind. Eng. Chem. Res. **57**, 8299-8307 (2018).

[23] C. Lv, P. Hao, Z. Yao, Y. Song, X. Zhang, and F. He, "Condensation and jumping relay of droplets on lotus leaf", Appl. Phys. Lett. **103**, 21601 (2013).

[24] R. Enright, N. Miljkovic, A. Al-Obeidi, C. V Thompson, and E.N. Wang, "Condensation on superhydrophobic surfaces: the role of local energy barriers and structure length scale", Langmuir **28**, 14424-14432 (2012).

[25] N. Miljkovic, D.J. Preston, R. Enright, and E.N. Wang, "Electric-field-enhanced condensation on superhydrophobic nanostructured surfaces", ACS Nano **7**, 11043-11054 (2013).

[26] R. Enright, N. Miljkovic, N. Dou, Y. Nam, and E.N. Wang, "Condensation on superhydrophobic copper oxide nanostructures", J. Heat Transf. **135**, 091304 (2013).

[27] Á.M. Soto, T. Maddalena, A. Fraters, D. Van Der Meer, and D. Lohse, "Coalescence of diffusively growing gas bubbles." J. Fluid Mech. **846**, 143 (2018).

[28] R. Iwata, L. Zhang, Z. Lu, S. Gong, J. Du, and E.N. Wang, "How Coalescing Bubbles Depart from a Wall", Langmuir **38**, 4371-4377 (2022).

[29] J. Straub, "Boiling heat transfer and bubble dynamics in microgravity", Advances in Heat Transfer 35, 57–172 (2001).

[30] A. Sielaff, D. Mangini, O. Kabov, M.Q. Raza, A.I. Garivalis, M. Zupančič, S. Dehaeck, S. Evgenidis, C. Jacobs, D. Van Hoof, O. Oikonomidou, X. Zabulis, P. Karamaounas, A. Bender, F. Ronshin, M. Schinnerl, J. Sebilleau, C. Colin, P. Di Marco, T. Karapantsios, I. Golobič, A. Rednikov, P. Colinet, P. Stephan, and L. Tadrist, "The multiscale boiling investigation on-board the International Space Station: An overview", Appl. Therm. Eng. **205**, 117932 (2022).

[31] O. Oikonomidou, S. Evgenidis, C. Argyropoulos, X. Zabulis, P. Karamaoynas, M.Q. Raza, J. Sebilleau, F. Ronshin, M. Chinaud, A.I. Garivalis, M. Kostoglou, A. Sielaff, M. Schinnerl, P. Stephan, C. Colin, L. Tadrist, O. Kabov, P. Di Marco, and T. Karapantsios, "Bubble growth analysis during subcooled boiling experiments on-board the international space station: Benchmark umage analysis", Adv. Colloid Interfac. **308**, 102751 (2022).

[32] M.S. Plesset and S.A. Zwick, "The growth of vapor bubbles in superheated liquids", J. Appl. Phys. **25**, 493-500 (1954).

[33] C.R. Anthony, P.M. Kamat, S.S. Thete, J.P. Munro, J.R. Lister, M.T. Harris, and O.A. Basaran, "Scaling laws and dynamics of bubble coalescence", Phys. Rev. Fluids **2**, 83601 (2017).

[34] M. Ohnishi, H. Azuma, and J. Straub, "Study on secondary bubble creation induced by bubble coalescence", Adv. Space Res. **24**, 1331-1336 (1999).

[35] F.H. Zhang and S.T. Thoroddsen, "Satellite generation during bubble coalescence", Phys. Fluids **20**, 022104 (2008).

[36] F. Blanchette and T.P. Bigioni, "Partial coalescence of drops at liquid interfaces", Nat. Phys. **2**, 254-257 (2006).

[37] P. Kumar Kirar, S.D. Pokale, K. Chandra Sahu, B. Ray, G. Biswas, "Influence of the interaction of capillary waves on the dynamics of two drops falling side-by-side on a liquid pool", Phys. Fluids **34**, 112114 (2022).

[38] M.K. Kim, H. Cha, P. Birbarah, S. Chavan, C. Zhong, Y. Xu, and N. Miljkovic, "Enhanced jumping-droplet departure", Langmuir **31**, 13452-13466 (2015).

[39] X. Yan, L. Zhang, S. Sett, L. Feng, C. Zhao, Z. Huang, H. Vahabi, A.K. Kota, F. Chen, and N. Miljkovic, "Droplet jumping: effects of droplet size, surface structure, pinning, and liquid properties", ACS Nano **13**, 1309-1323 (2019).

[40] K. Wang, Q. Liang, R. Jiang, Y. Zheng, Z. Lan, and X. Ma, "Self-enhancement of droplet jumping velocity: the interaction of liquid bridge and surface texture", RSC Adv. **6**, 99314-99321 (2016).

[41] H. Lamb, *Hydrodynamics* (University Press, 1924).

[42] M. Minnaert, The London, Edinburgh, and Dublin Philosophical Magazine and Journal of Science **16**, 235 (1933).

[43] Levich BV, "Bubble motion at high Reynolds numbers", Zh. Eksp. Teoret. **19**, 18 (1949).

[44] B. Jingliang, L. Xipeng, and D.M. Christopher, "Effects of bubble coalescence dynamics on heat flux distributions under bubbles", AIChE Journal **59**, 1735-1745 (2013).

PLEASE CITE THIS ARTICLE AS DOI: 10.1063/5.0138200

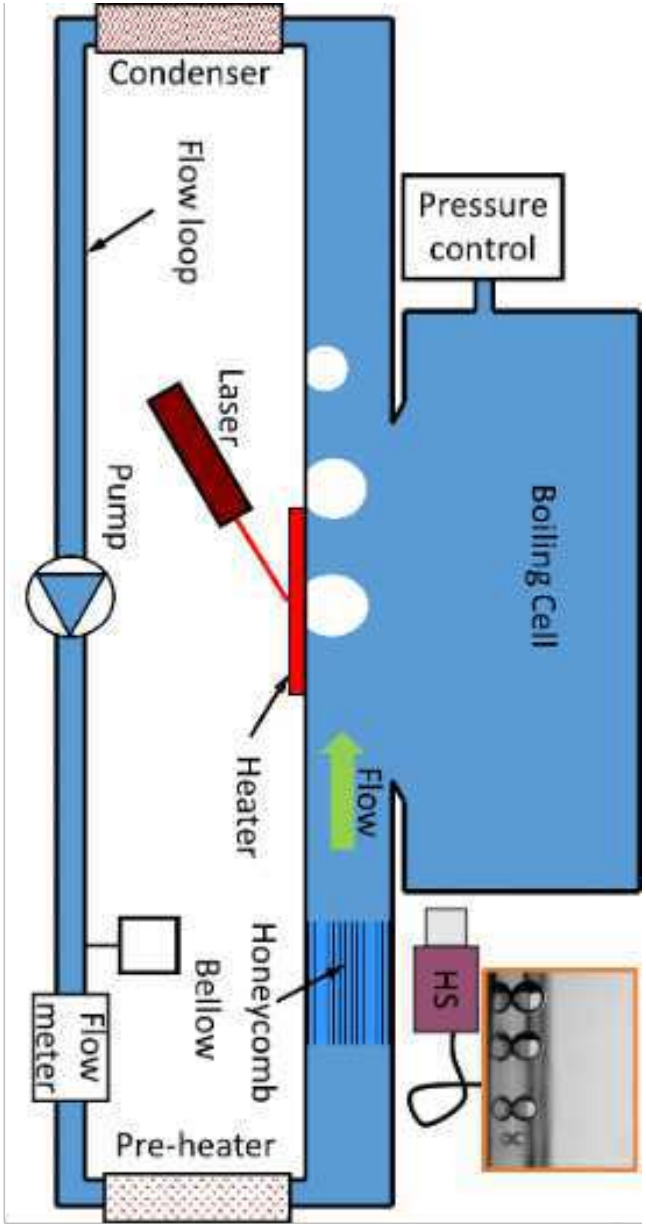

PLEASE CITE THIS ARTICLE AS DOI: 10.1063/5.0138200

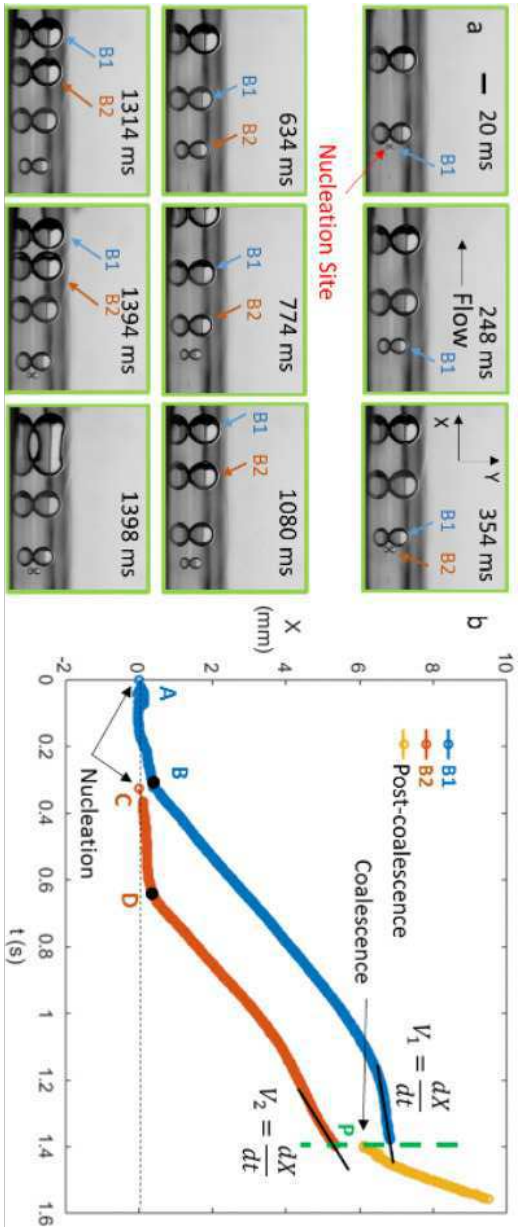

Physics of Fluids

PLEASE CITE THIS ARTICLE AS DOI: 10.1063/5.0138200

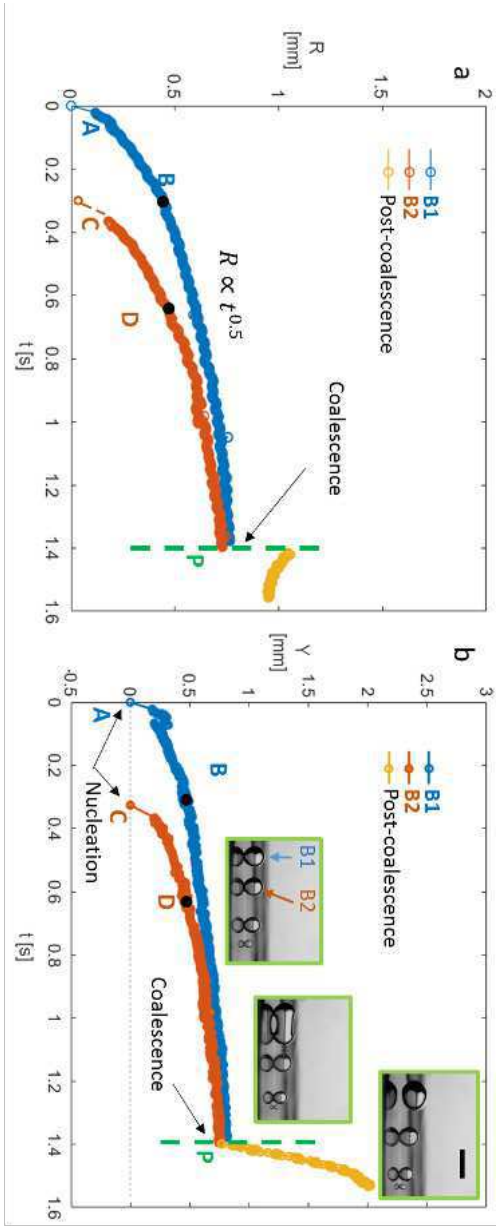

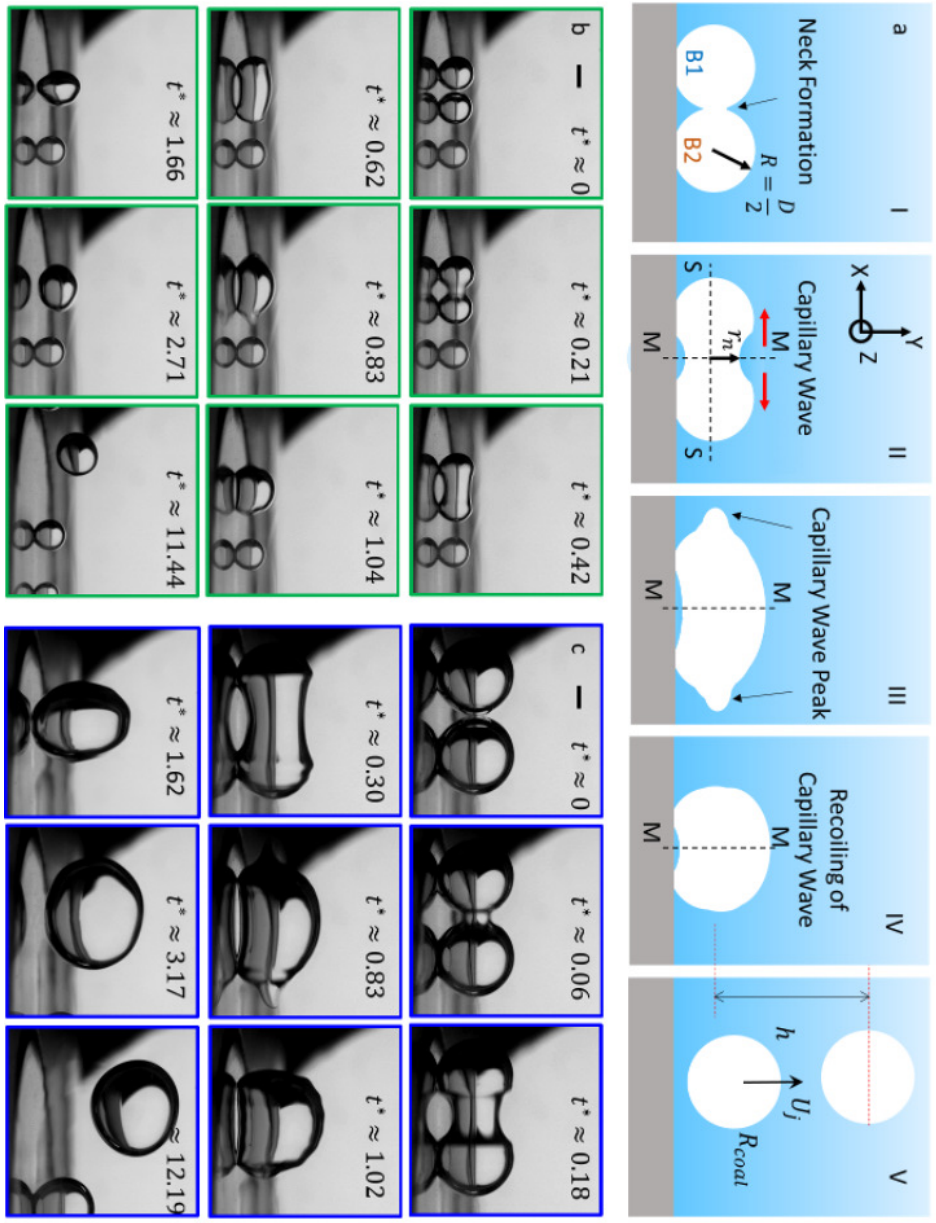

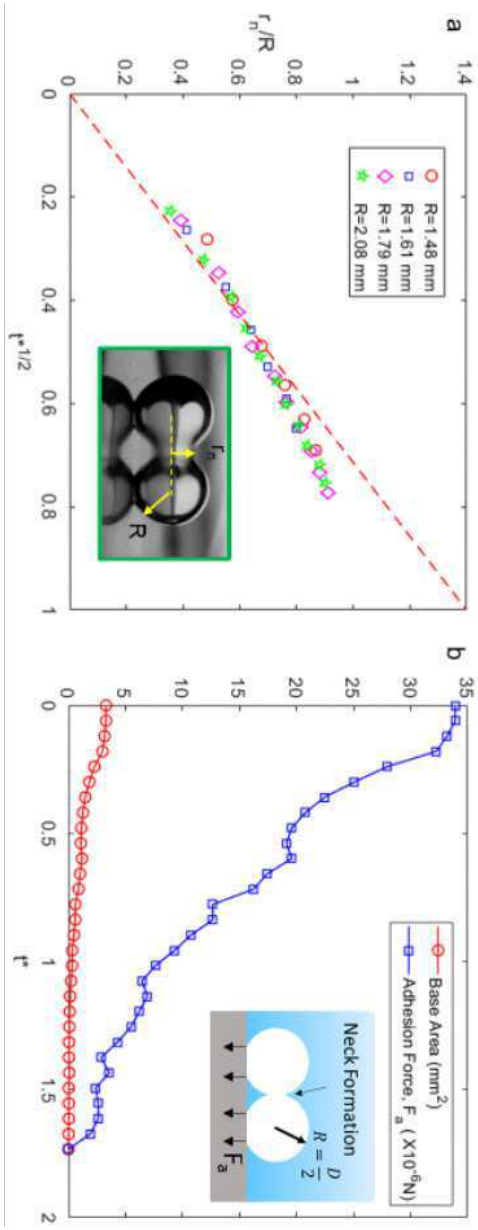

Physics of Fluids

PLEASE CITE THIS ARTICLE AS DOI: 10.1063/5.0138200

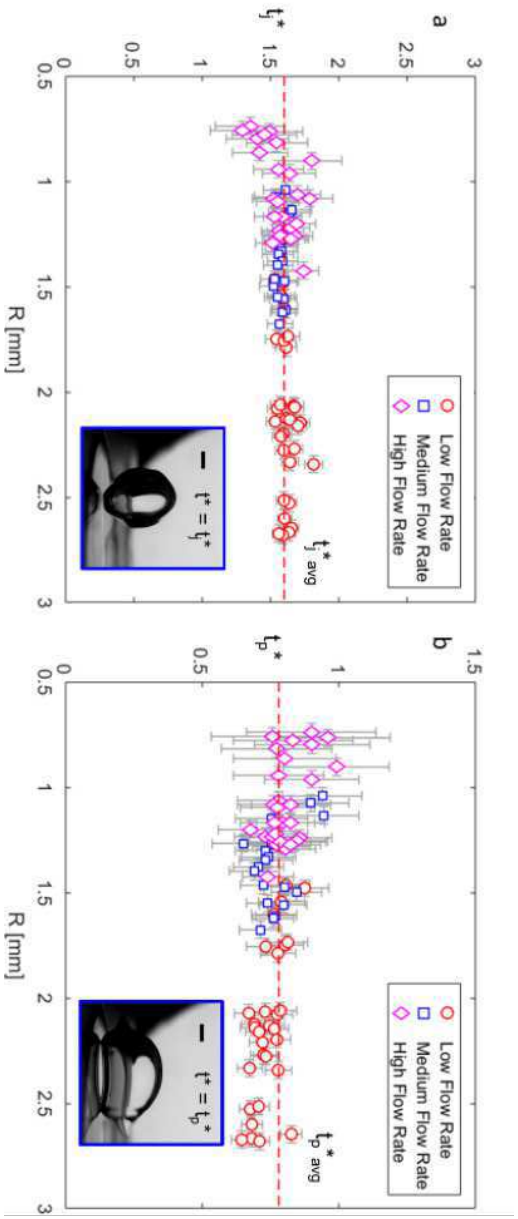

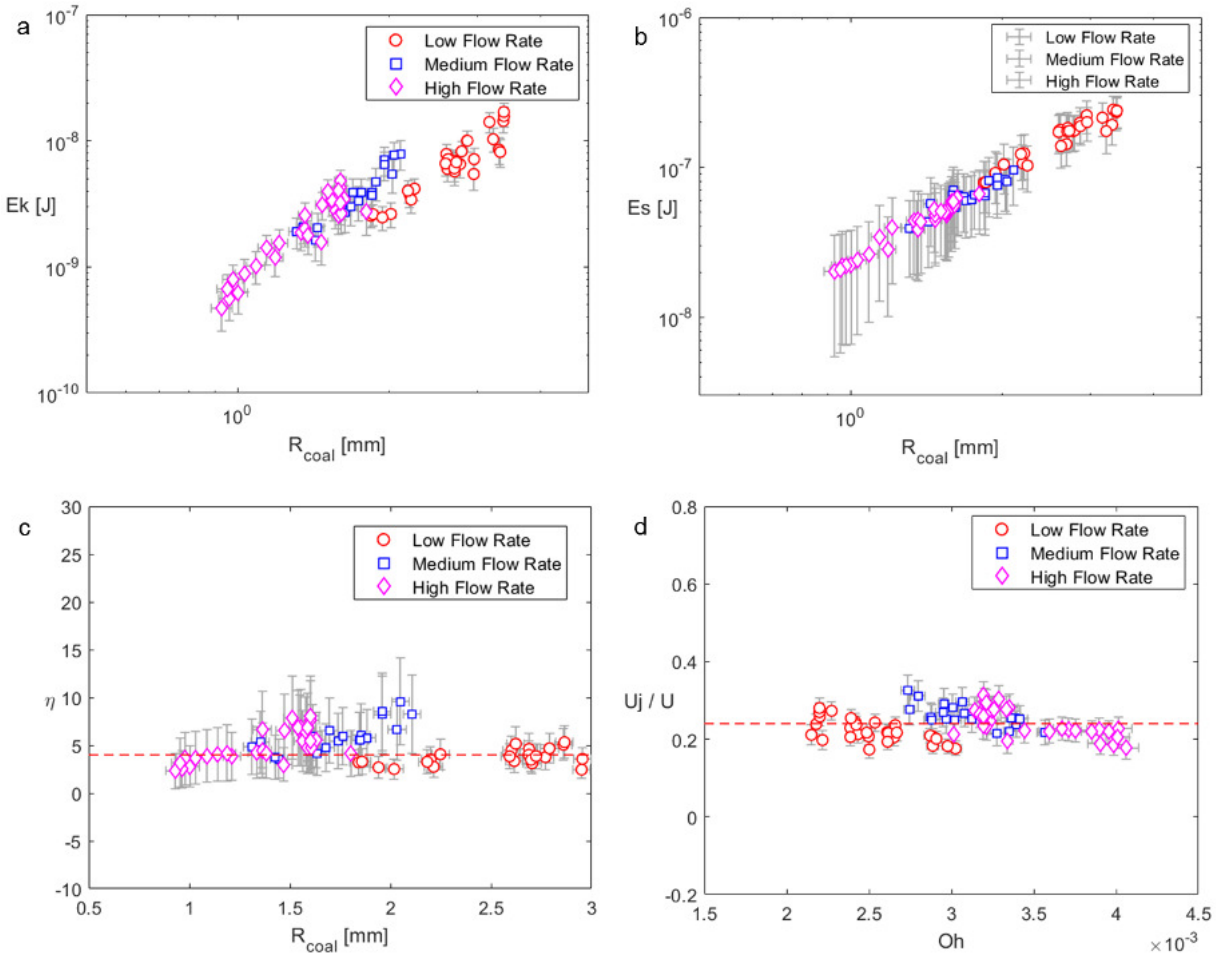

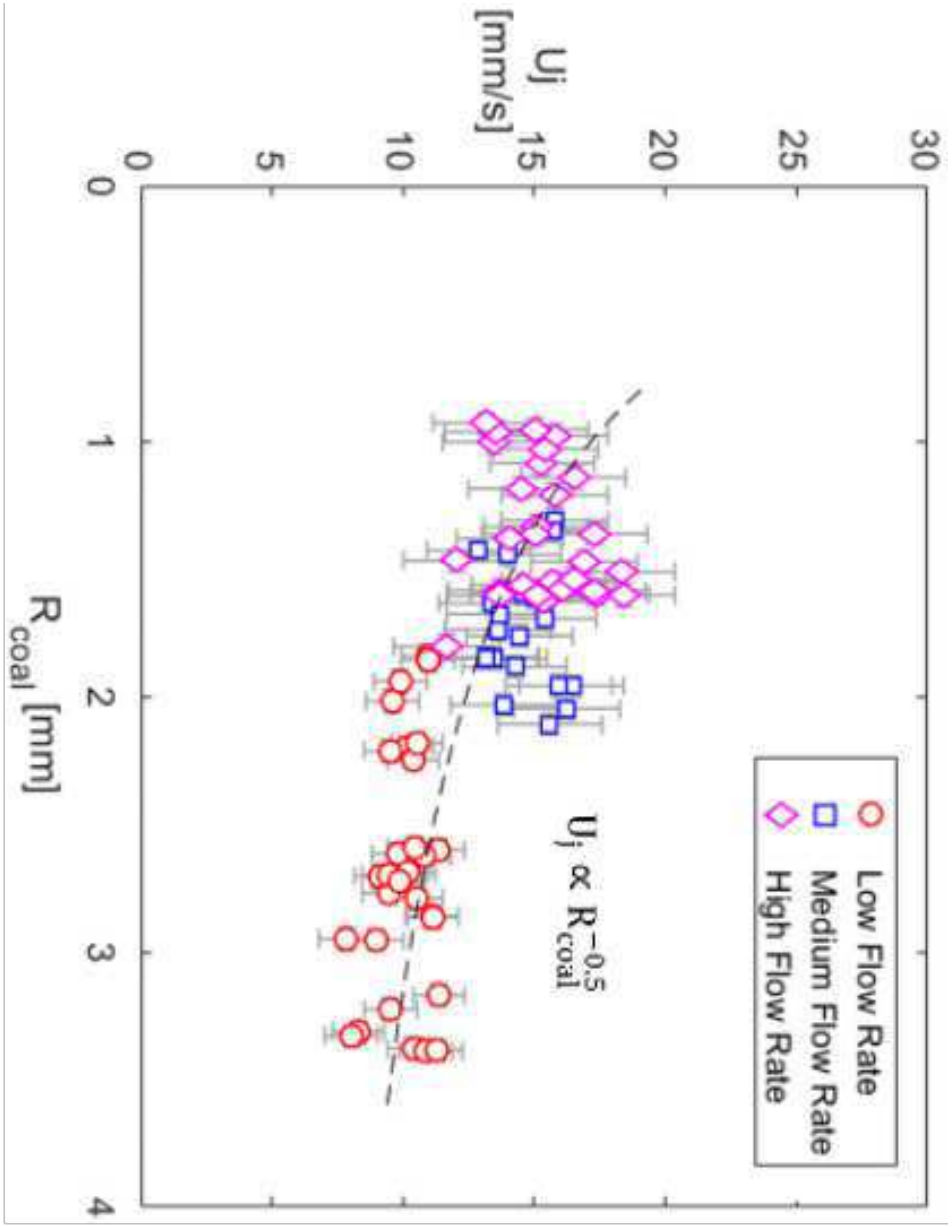

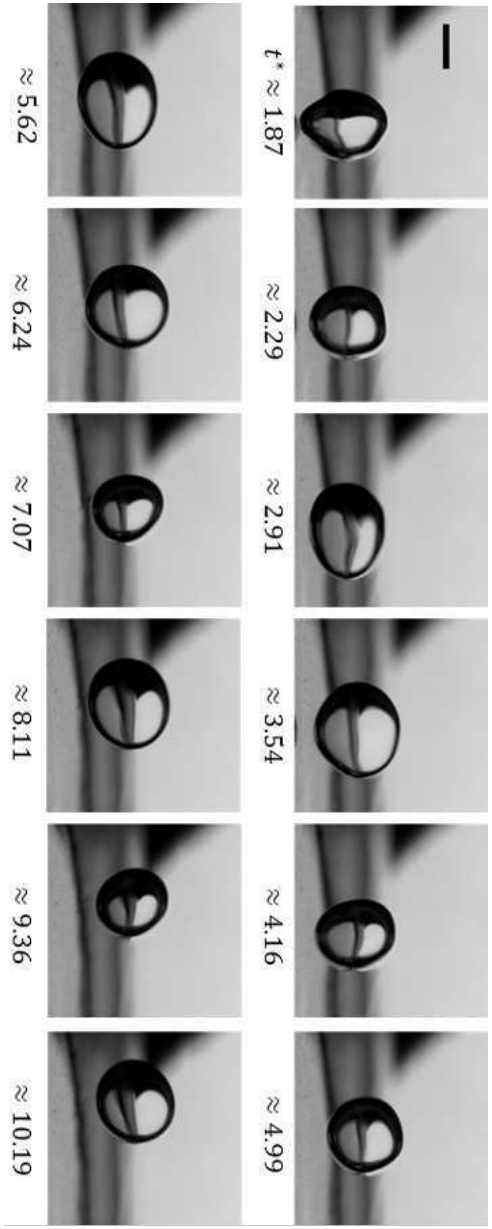

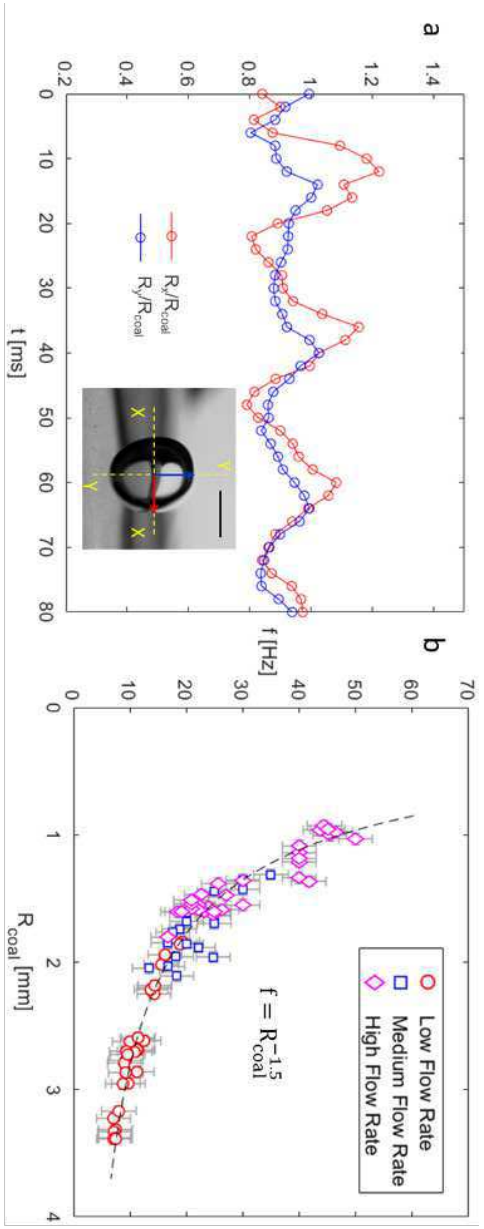

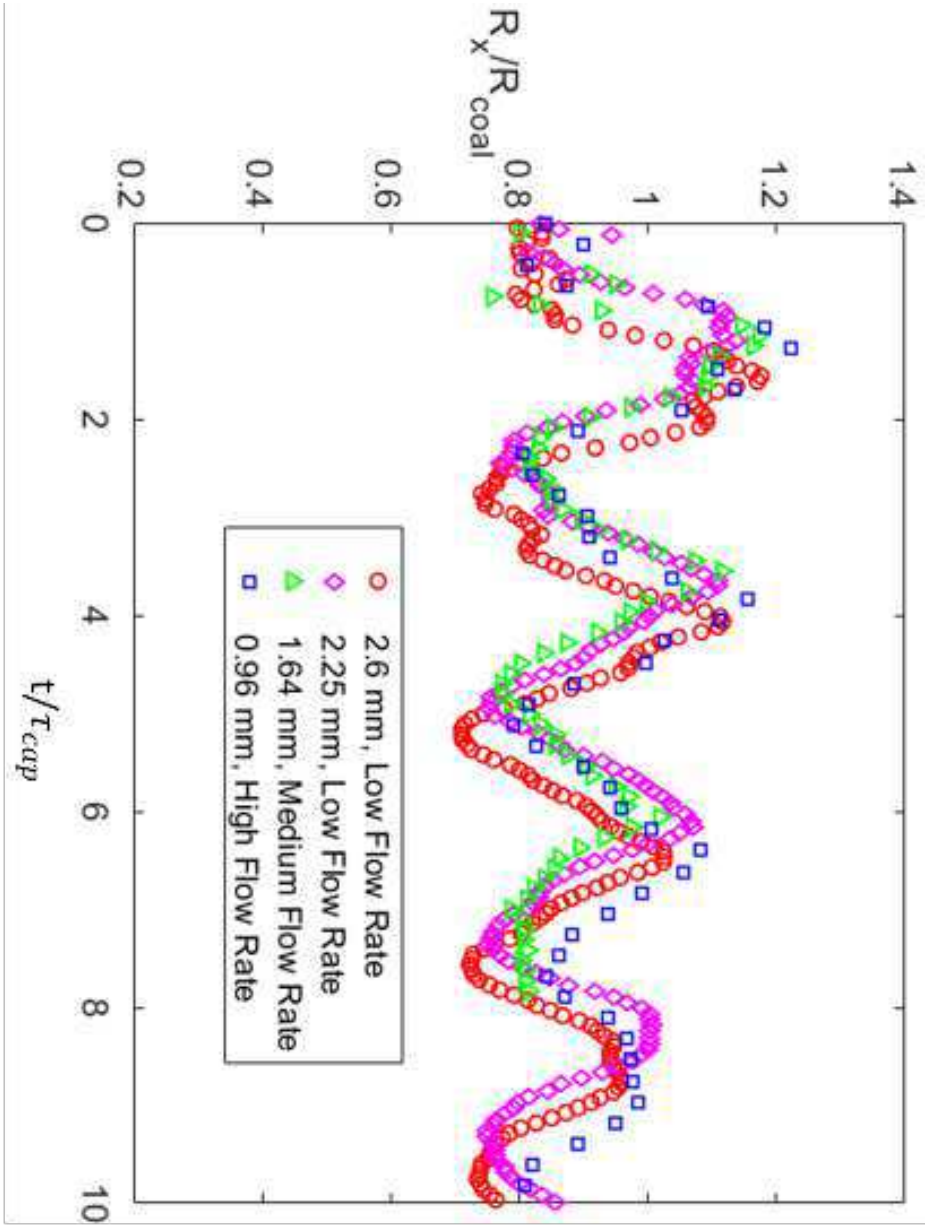

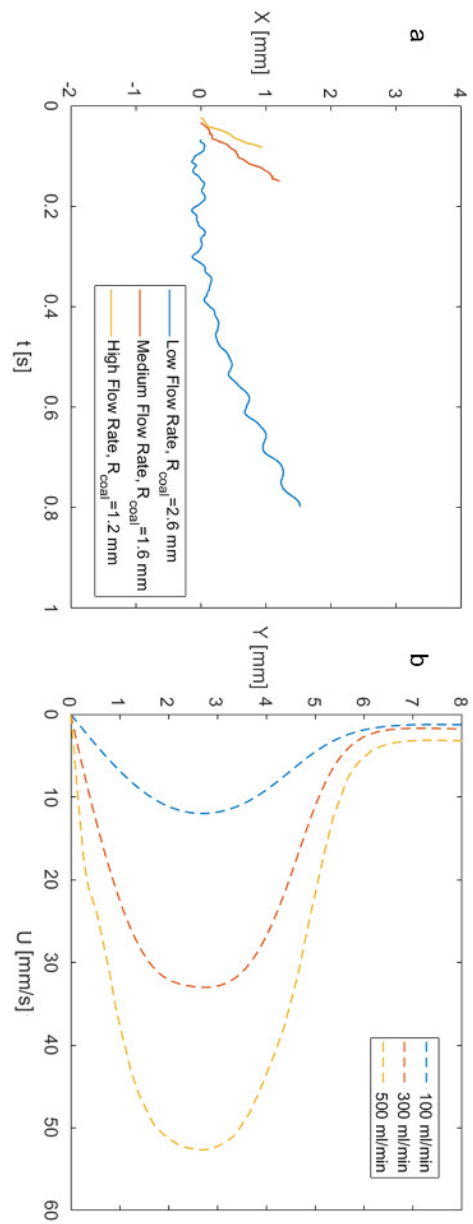

PLEASE CITE THIS ARTICLE AS DOI: 10.1063/5.0138200

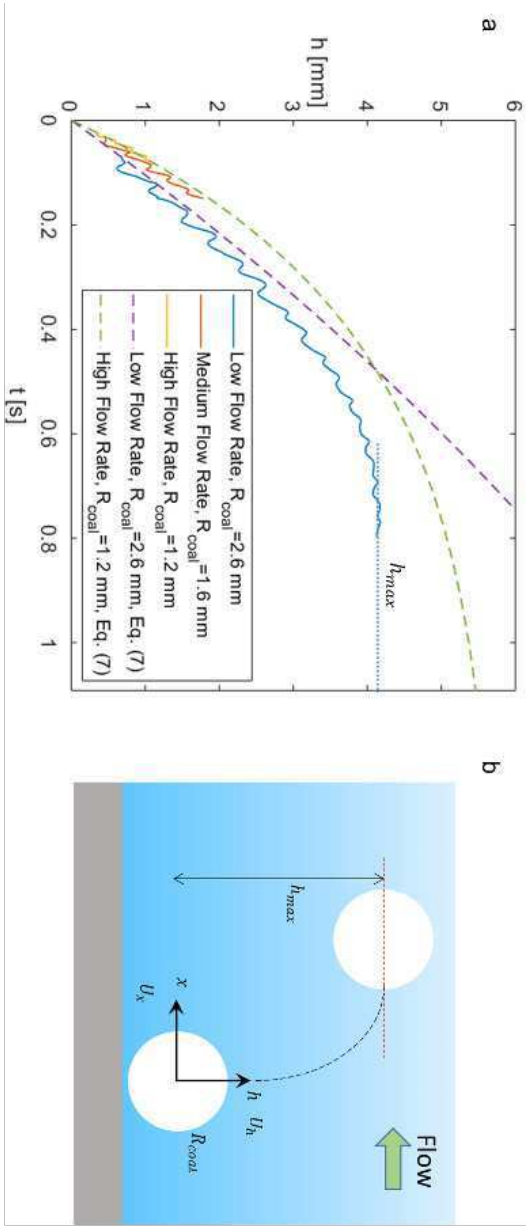

PLEASE CITE THIS ARTICLE AS DOI: 10.1063/5.0138200